Supplementary Figures

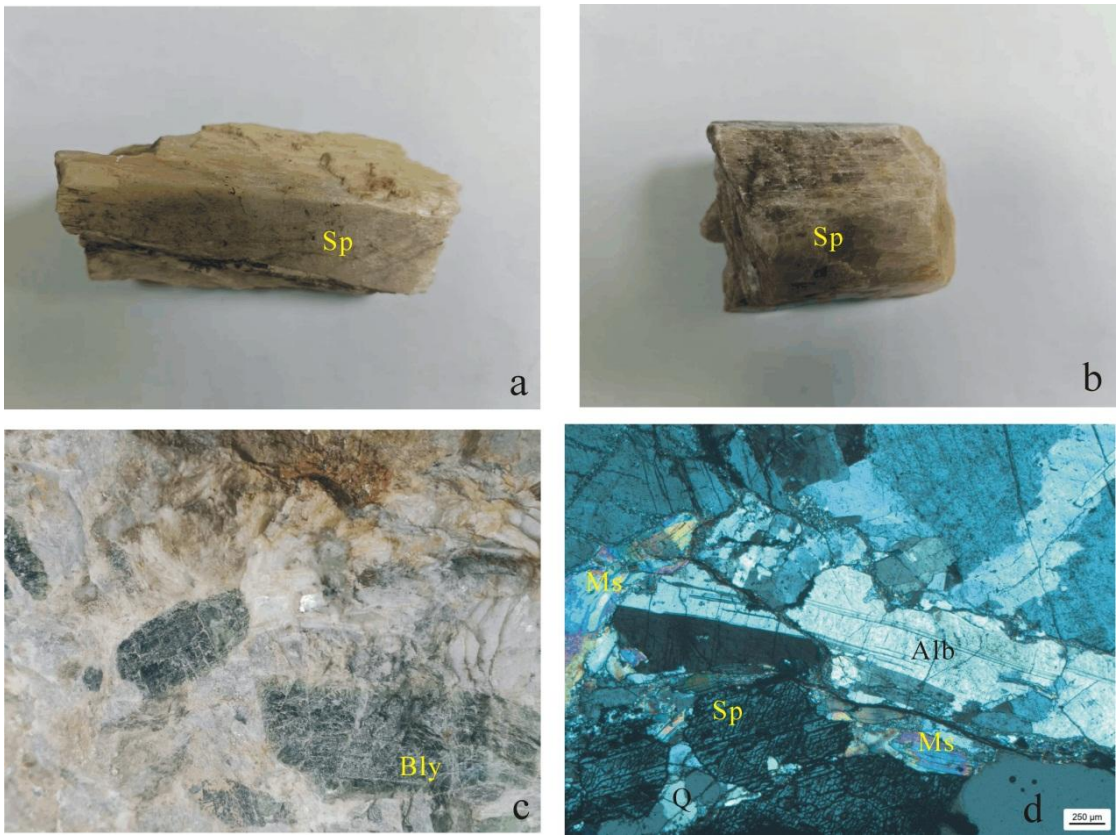

Supplementary Fig. 1 Specimen photos of the ore from the Kôhe-Jamânak rare metal deposit in Afghanistan. a, b-spodumene crystal; c-beryl crystal; d-micro photo of the ore. Sp-spodumene, Bly-beryl; Alb-albite; Ms-muscovite.

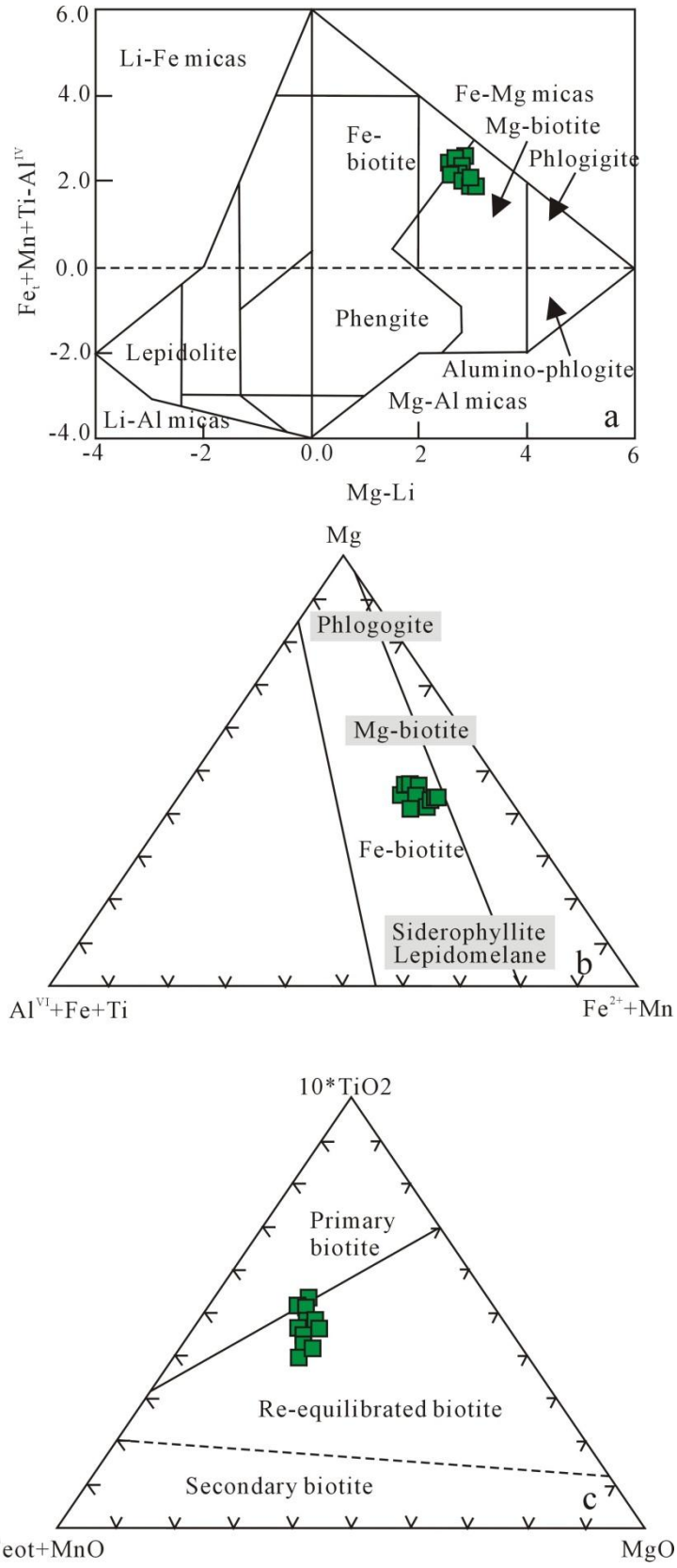

Supplementary Fig. 2 Classification diagrams of the biotite from the gabbroic diorite.

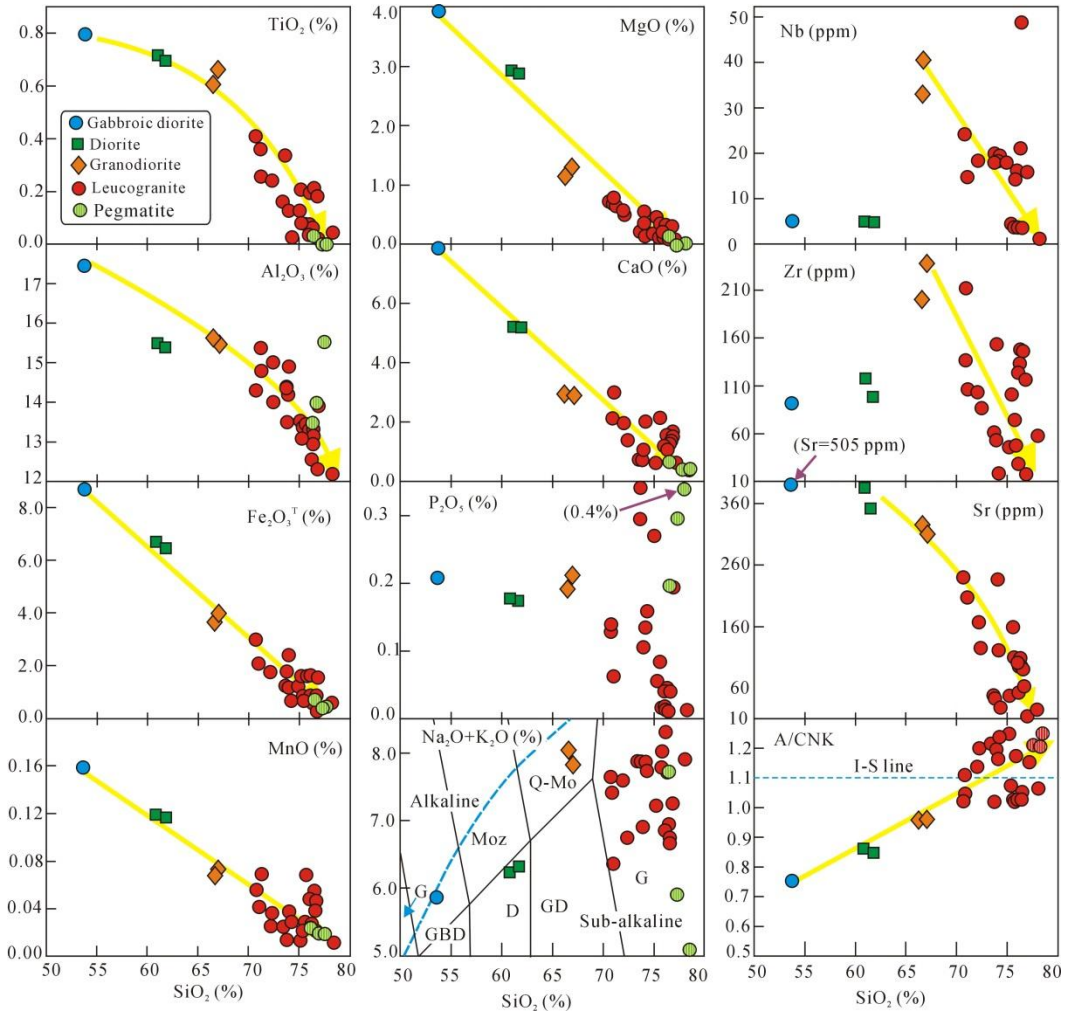

Supplementary Fig. 3 Harker diagram of the (gabbroic) diorites, granodiorite, leucogranite and pegmatites (Data from Fasial et al., 2016 are also included).

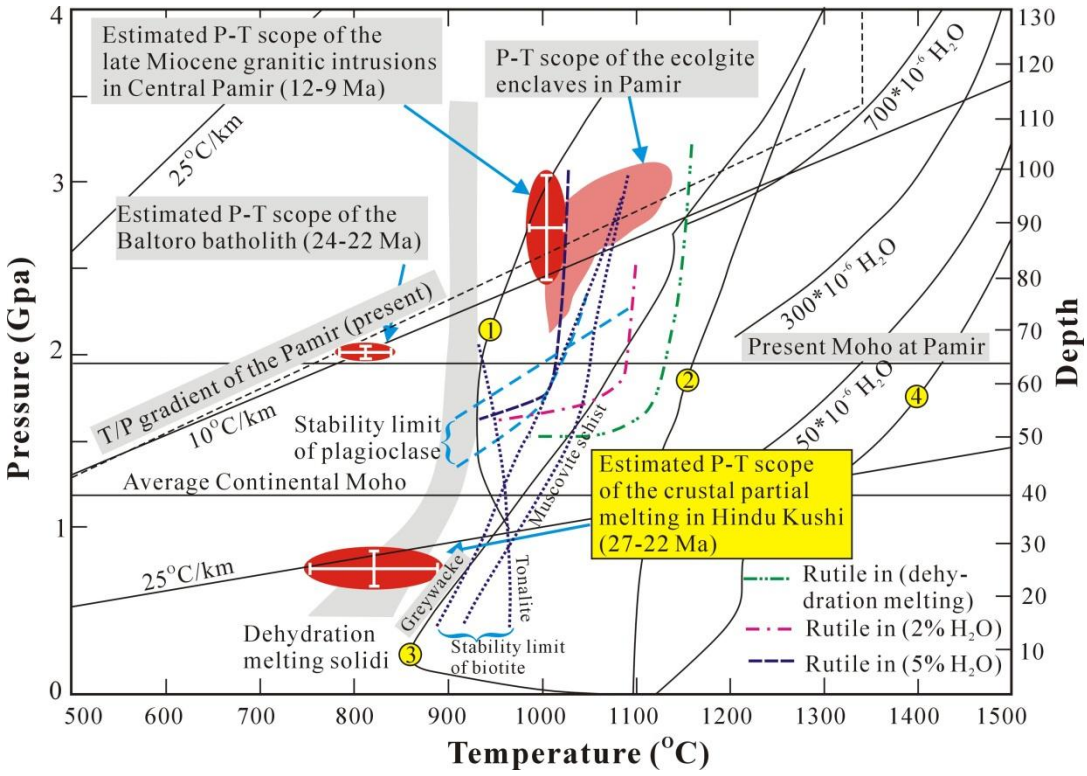

Supplementary Fig. 4 P-T estimation of the partial melting of the 24-22 Ma Baltoro batholith, 27-22 Ma granite-pegmatites and the 12-9 Ma syenite-granites. ① H_2O saturated melt-solid line of basalt melting (after Falloon et al., 1989, cited from Leeman and Hary, 1993); ② melt-solid line of dry basalt melting (Thompson, 1975, cited from Leeman and Hary, 1993); ③ H_2O saturated melt-solid line of the depleted peridotite; ④ melt-solid line of the dry depleted peridotite (Asimow et al., 2004). The plagioclase stability field (partial melting of muscovite schist and tonalite) and the melt-solid line of dehydration partial melting of muscovite schist, tonalite and meta-greywacke are from Patino Douce et al. (1998) and Hacker et al. (2005). The P-T scope of the eclogites from the lower crust, the present P-T gradient of Pamir, present Moho depth of Pamir and the average Moho depth of continents are from

Hacker et al. (2005). The solid-melt line of the rutile is from Xiong et al. (2006). The P-T scope of the eclogite facies metamorphism at NE Pamir is from Li et al. (2020).

References cited in the Supplementary Figures

Asimow, P.D., Dixon, J.E., Langmuir, C.H., 2004. A hydrous melting and fractionation model for mid-ocean ridge basalts: application to the Mid-Altantic Ridge near the Azores. Geochemistry, Geophysic and Geosystem 5, 1-24.

Chauvel, C., Lewin, E., Chrpentier, M., Arndt, N., Marini, J.C., 2008. Role of recycled oceanic crust and sediment in generation of the Hf-Nd mantle array. Nature 1, 64-67.

Faisal, S., Larson, K.P., King, J., Cottle, J.M., 2016. Rifting, subduction and collisional records from pluton petrogenesis and geochronology in the Hindu Kush, NW Pakistan. Gond. Res. 35, 286-304.

Hacker, B., Luffi, P., Lutkov, V., 2005. Near-ultrahigh pressure processing of continental crust: Miocene crustal xenoliths from the Pamir. Journal of Petrology 46, 1661-1687.

Ke, S., Teng, F., Li, S., Gao, T., Liu, S., He, Y., Mo, X., 2016. Mg, Sr, and O isotope geochemistry of syenites from northwest Xinjiang, China: Tracing carbonate recycling during Tethyan oceanic subduction. Chem. Geol. 437, 109-119.

Ridolfi, F., 2021. Amp-TB2: An Updated Model for Calcic Amphibole Thermobarometry. Minerals 11, 2-9.

Li, Y., Robinson, A. C., Lapen, T. J., Righter, M., Stevens, M. K., 2020. Muztaghata

Dome Miocene eclogite facies metamorphism: A record of lower crustal evolution of the NE Pamir. Tectonics 38, e2019TC005917.

Leeman, W.P. and Hary, D.L., 1993. A binary source model for extension related magmatism in the Great Basin, Western North Amierica. Science 262, 1550-1554.

Patino Douce, A.E., McCarthy, T.C., 1998. Melting of crustal rocks during continental collision and subduction. In: Hacker, B.E., et al eds., When continents collide: geodynamics and geochemistry of ultrahigh-pressure rocks. Dordrecht: Kluwer Academic, 27-55.

Xiong, X.L., Ada,, J., Green, T.H., 2005. Rutile stability and rutile/melt HFSE portioning during partial melting of hydrous basalt: implication for TTG genesis. Chemical Geology 218, 339-359.